NANOSYSTEMS:
PHYSICS, CHEMISTRY, MATHEMATICS

Original article

Talanov V.M., et al. *Nanosystems: Phys. Chem. Math.*, 2023, **14** (2), 208–215.
http://nanojournal.ifmo.ru
DOI 10.17586/2220-8054-2023-14-2-208-215

Symmetry-based prediction of the type-II multiferroics with pyrochlore structure

Valeriy M. Talanov[1,a], Mikhail V. Talanov[1,2,b], Vladimir B. Shirokov[1,2,3,c]

[1]Platov South-Russian State Polytechnic University, Novocherkassk, Russia

[2]Southern Federal University, Rostov-on-Don, Russia

[3]Southern Scientific Center of Russian Academy of Sciences, Rostov-on-Don, Russia

[a]valtalanov@mail.ru, [b]mvtalanov@gmail.com, [c]shirokov.ssc@gmail.com

Corresponding author: Valeriy M. Talanov, valtalanov@mail.ru

PACS 05.70.Fh; 61.50.Ah; 61.50.Ks; 61.66.Fn

ABSTRACT Based on the symmetry related concept of the group theory we predict two structures with enantiomorphic space groups P_I4_3 and P_I4_1. These phases arise as a result of spin ordering on 16d Wyckoff position in crystals with space group $Fd\bar{3}m$. It is shown that P_I4_3 and P_I4_1 hypothetical magnetic structures are multiferroics of type II. The ferroelectric polarization emerges through a mechanism of the hybrid improper ferroelectricity allowing trilinear coupling of polarization and two other antiferromagnetic order parameters. In addition to improper ferroelectricity, the symmetry analysis proves the possible coexistence of other improper ferroic orders including orbital, ferroelastic, ferroelastoelectric, ferrobielastic, optical, ferroaxial, ferrotoroidic, gyrotropic and other crystal freedom degrees.

KEYWORDS spin order, multiferroics, improper ferroelectrics, trilinear coupling, multi-order state, secondary ferroics.

ACKNOWLEDGEMENTS The reported study was funded by Russian Science Foundation (RSF)-research projects No. 22-22- 00183, https://rscf.ru/project/22-22-00183/

FOR CITATION Talanov V.M., Talanov M.V., Shirokov V.B. Symmetry-based prediction of the type-II multiferroics with pyrochlore structure. *Nanosystems: Phys. Chem. Math.*, 2023, **14** (2), 208–215.

1. Introduction

Magnetoelectric multiferroics demonstrate both magnetic and ferroelectric order with the mutual influence of the corresponding properties on each other. Thus, the electric field control of magnetization or vice versa magnetic field tunable electric polarization are possible that opens up a wide range of practical applications including magnetic field sensors, electrically tunable microwave resonators, random access multi-state memories and many others [1]. The classification by Khomskii distinguishes two types of multiferroics [2]. In a type-I multiferroics, ferroelectricity and magnetism appear independently and, most often, different subsystems and ions are responsible for them. Classical examples are oxides with the perovskite structure $BiFeO_3$ and $BiMnO_3$, in which ferroelectricity is due to Bi^{3+} ions with a lone pair of electrons in the A sublattice, and magnetism is associated with ions with a partially filled d shell in the B sublattice [3–5]. The magnetic and ferroelectric degrees of freedom in these systems are coupled, but the magnetoelectric coefficients are rather low that hinders many applications. In a type-II multiferroics, ferroelectric polarization arises due to magnetic ordering, which usually leads to a stronger magnetoelectric interaction. Typical examples are $TbMnO_3$ [6], $Tb_2Mn_2O_5$ [7] and many other structures, where spin order induces electrical polarization [8].

Approaches to the design of magnetoelectric materials and corresponding nanosystems differ significantly for type -I and type-II multiferroics. For a long time, it was believed that magnetism and ferroelectricity in one substance should not coexist due to the so-called "d^n–d^0 separation" [9]. The meaning of this rule is very simple: substances containing partially filled d-shells are magnetic, while substances with an unfilled d^0-configuration will be non-magnetic but may turn out to be ferroelectric as a result of the pseudo Jahn-Teller effect (similar to $BaTiO_3$) [10]. Thus, there is a contradictory requirement for the electronic structure of the single ions responsible for ferroelectricity and magnetism.

One of the main directions in solving the problem of "d^n–d^0 separation" was the design of materials in which different sublattices were "responsible" for magnetic or ferroelectric properties. Such materials are type-I multiferroics or ferromagnetics [11]. In addition to the already mentioned $BiFeO_3$ and $BiMnO_3$, type-I multiferroics include $PbFe_{2/3}W_{1/3}O_3$, $PbFe_{1/2}Nb_{1/2}O_3$, various solid solutions based on them, as well as many other complex perovskites of the Pb(B'B'')O_3 type. In these cases, magnetic and ferroactive ions occupy different sublattices of the perovskite structure and/or are randomly mixed in one of the sublattices [3–5].

Another approach to the creation of magnetoelectric materials are composites (two-phase multiferroics) based on piezoelectric and magnetostrictive components, which often belong to different structural types, as, for example, in the case of widely studied nano- and bulk composites based on $PbZr_{0.5}Ti_{0.5}O_3$ (perovskite) and $NiFe_2O_4$ (spinel) and many

others [12]. Under the action of a magnetic field, the ferrite is deformed due to magnetostriction. This deformation, in turn, induces the appearance of an electric charge at the boundaries of the ferroelectric phase as a result of the direct piezoelectric effect. Thus, the magnetoelectric interaction is carried out due to the magnetic subsystem, which has been confirmed in various forms of connectivity of the mechanical and ferroelectric components of composites: mixed, layered, etc. [12].

In recent years, a new line of research has appeared in the field of creating the multiferroics. This line is associated with the discovery of a hybrid mechanism of improper ferroelectricity in the superlattices of various perovskites, for example, $PbTiO_3/SrTiO_3$ [13–16]. The polarization is possible due to the interaction of several nonferroelectric order parameters (in the case of the above superlattices, these are different types of oxygen octahedra tilts), which are described by a trilinear term of the $\eta_1\eta_2 P$ form (where η_1, η_2 are nonpolar distortions, and P is polarization) in the thermodynamic potential [17]. Later, hybrid improper ferroelectricity was also discovered in single-phase materials, including ordered perovskites [17–20], Ruddlesden–Popper phases [16, 19–27], molecular perovskites [28, 29], metal-organic frameworks [23] and other materials, including multiferroics (for example, [16,30]). Thus, the problem of "d^n–d^0 separation" can also be solved by creating artificial nanosystems - superlattices consisting of magnetic nonpolar layers, in which polarization occurs as an integral effect.

In the case of type-II multiferroics, the occurrence of ferroelectric polarization is due to magnetic ordering, which leads to the loss of the inversion center. In this case, the problem of "d^n–d^0 separation" is not relevant. To date, the main microscopic mechanisms of violation of the inversion center because of the specific geometry of both collinear and noncollinear spin-ordered structures have been identified [3,31]. Thus, in collinear magnetic structures with different types of magnetic ions (for example, chains of nonequivalent spins directed alternately downward - upward), the occurrence of polarization is caused by the mechanism of exchange striction [33]. In noncollinear magnets, magnetically induced ferroelectricity is possible due to the spin-current mechanism or reverse Dzyaloshinsky-Moriya model for canted spins or spiral magnetic structures [34] including cycloid and transverse conical ones [32].

One of the promising atomic architectures for the implementation of various magnetic orders and, as a result, magnetically induced ferroelectricity is the pyrochlore lattice [35,36], which is a part of the structures of pyrochlores, spinels, and C15 Laves phases (Fig. 1).

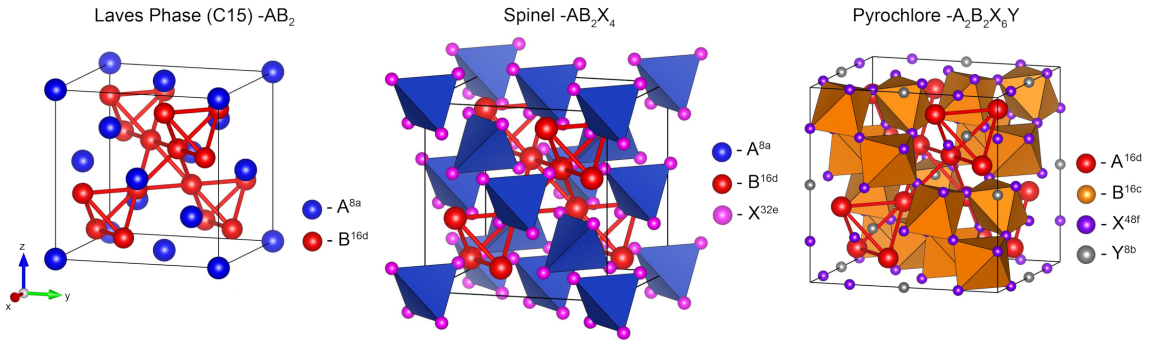

FIG. 1. Main structural types of materials with pyrochlore sublattice. Pyrochlore sublattice in Laves phases (C15) AB_2 (a), normal spinel AB_2X_4 (c), $A_2B_2X_6Y$ pyrochlore (c). In all figures, this sublattice is shown in red

To date, a huge number of various magnetic materials with a pyrochlore lattice are known, which are characterized by a diversity of spin-ordered structures [32, 35]. This lattice is a platform for the implementation of various types of competing and coexisting interactions, which is due to strong geometric frustration. Materials with pyrochlore lattices tend to exhibit a very complex relationship of interacting structural, orbital, charge, and spin degrees of freedom. The nature of such multi-order determining the unique physical properties of this class of materials cannot be understood without profound knowledge of group-theoretical symmetry principles. The aim of this work is to make a group-theoretical prediction of some types of the complex multi-orders, similar to improper ferroelectricity in type II multiferroics, and generated by ordering the spins of magnetic cations on the pyrochlore lattice.

2. Methods

We will consider the case of the formation of spin-ordered structures that is not accompanied by the splitting of the $16d$ Wyckoff positions of the $Fd\bar{3}m$ space group. If we take this limitation, within the framework of Landau phase transition theory, it is sufficient only to consider the magnetic order parameters (OPs) with two propagation vectors $k = (0, 0, 0)$ and $k = (0, 0, 1)$. For irreducible representations (*irreps*) of these wave vectors, the magnetic representations are as follow:

$$T_{mag} = \left(m\Gamma_2^+\right) \oplus \left(m\Gamma_3^+\right) \oplus \left(m\Gamma_5^+\right) \oplus 2\left(m\Gamma_4^+\right) \quad for \quad k = (0, 0, 0), \tag{1}$$

TABLE 1. Theoretically predicted structures of the type-II multiferroics derived from cubic pyrochlore lattice without splitting of the initial 16d Wyckoff crystallographic positions of $Fd\bar{3}m$ space group

Primary OPs	Secondary OPs	Magnetic space group	Basis vectors	Origin	Size
	$\Gamma_1^+(a)$				
	$\Gamma_1^-(a)$	P_I4_3			
$mX_3\ (0,0;0,0;a,0)$	$\Gamma_3^-(0,a)$	(No. 78.24)	(1/2,1/2,0)		
$mX_4\ (0,0;0,0;a,0)$	$\Gamma_4^-(0,0,a)$	UNI:	(-1/2,1/2,0)	(-3/8,3/8,0)	2
	$\Gamma_3^+(a,0)$	$P4_3.1'_I[I4_1]$	(0,0,1)		
	$\Gamma_4^+(0,0,a)$				
	$\Gamma_1^+(a)$				
	$\Gamma_1^-(a)$	P_I4_1			
$mX_3\ (0,0;0,0;0,a)$	$\Gamma_3^-(0,a)$	(No. 76.12)	(1/2,1/2,0)		
$mX_4\ (0,0;0,0;0,a)$	$\Gamma_4^-(0,0,a)$	UNI:	(-1/2,1/2,0)	(-1/8,1/8,0)	2
	$\Gamma_3^+(a,0)$	$P4_1.1'_I[I4_1]$	(0,0,1)		
	$\Gamma_4^+(0,0,a)$				

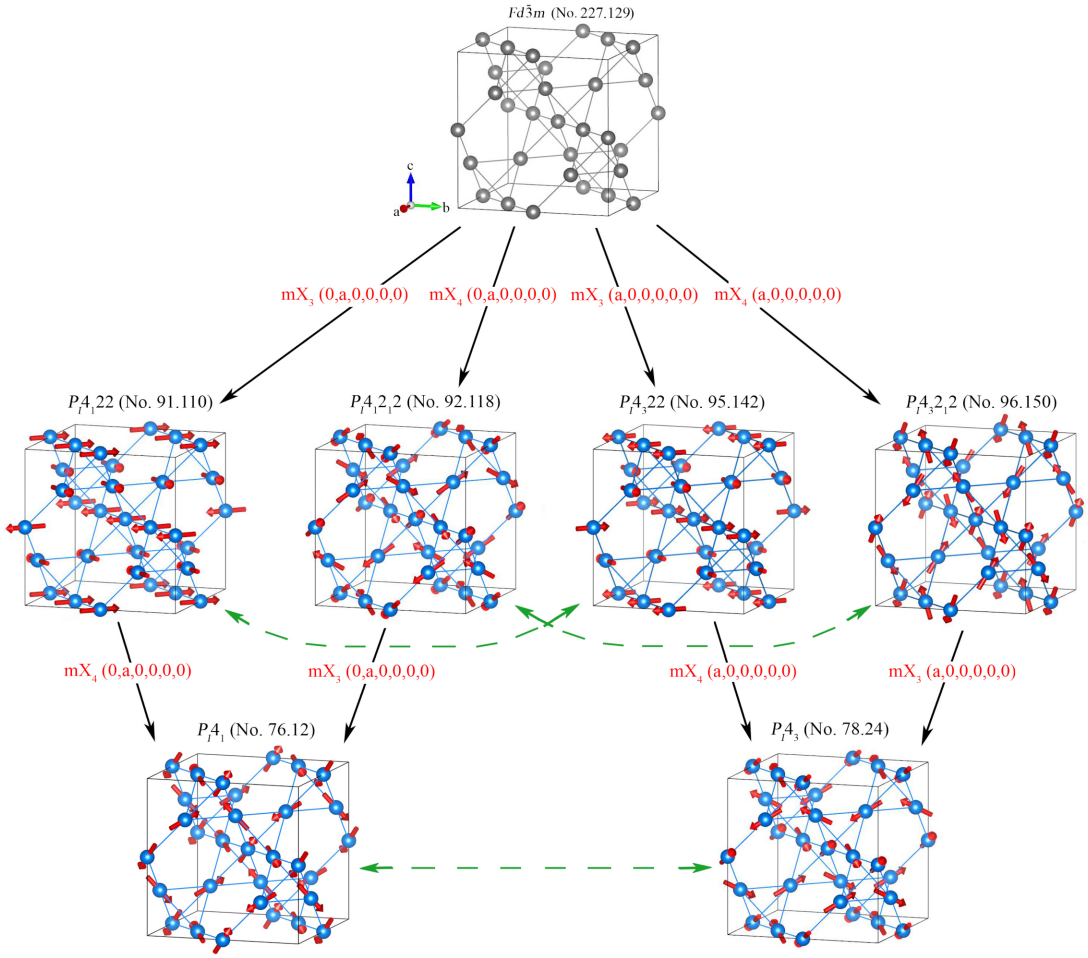

FIG. 2. Symmetric ways of formation of enantiomorphic structures with space groups P_I4_3 and P_I4_1 from the initial symmetry group $Fd\bar{3}m$. The OPs that generate transformations of structures are marked in red. Enantiomorphic pairs of structures are connected by green dotted arrows

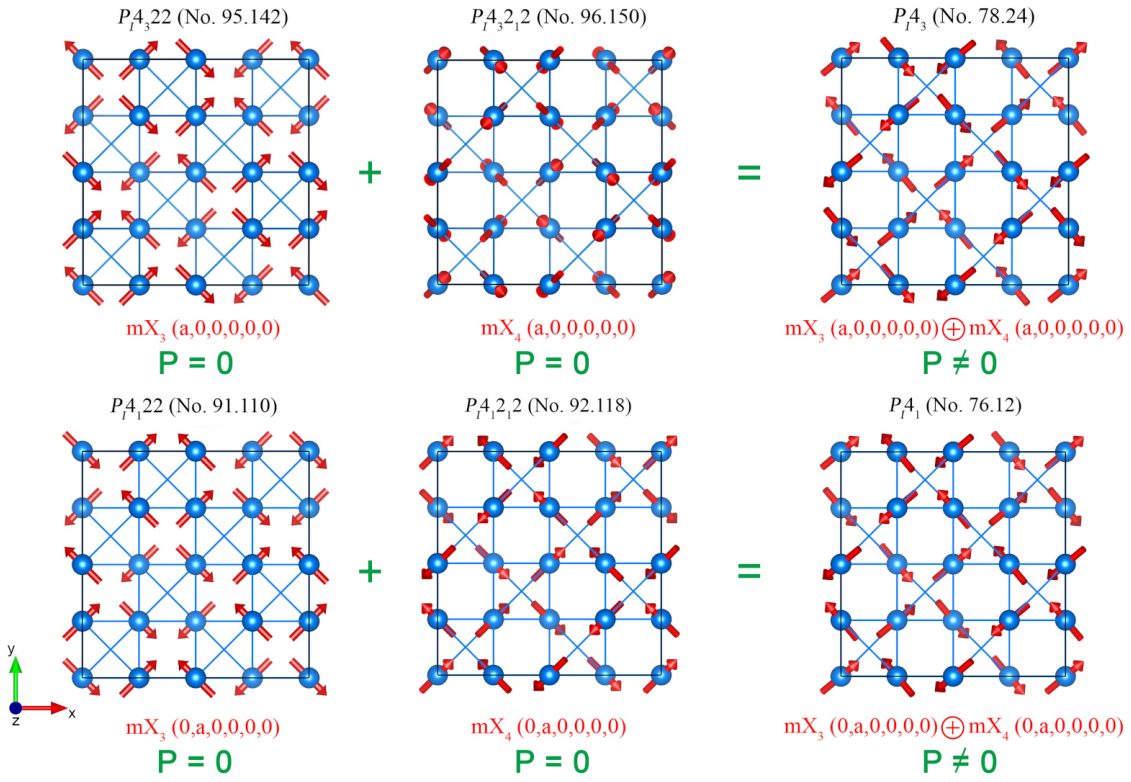

FIG. 3. Mechanism of the spin-induced polarization formation via trilinear coupling on the examples of an improper ferroelectric phases with space groups P_I4_3 (No. 78.24) and P_I4_1 (No. 76.12)

$$T_{mag} = (mX_3) \oplus 2\,(mX_4) \oplus (mX_1) \oplus 2(mX_2) \quad for \quad k = (0,0,1), \tag{2}$$

The compositions of the magnetic representations (1 and 2) determine the variety of magnetically ordered phases, possible types of phase diagrams and physical properties.

At present, some group-theoretical tasks of the magnetic phase transitions theory can be solved using computer programs (ISOTROPY Software Suite [37] and Bilbao Crystallographic Server [38]). In our work, we used ISODISTORT [37], k-Subgroupsmag/Get_mirreps [38], MAGMODELIZE programs [38]. Magnetic structure visualization was made by VESTA [39].

3. Results and discussion

According to our calculations, the magnetic representations (1 and 2) determine the possibility of the existence of 25 phases [32]. In the context of possible multiferroic phases, we underline two structures P_I4_3 (No. 78.24) and P_I4_1 (No. 76.12) which are induced by two OPs transformed by *irreps* mX_3 and mX_4 (with different OPs direction for these phases). Table 1 shows the sets of OPs that determine the magnetic structure, magnetic space group (Belov–Neronova–Smirnova [40] and new unified (UNI) [41] designation), secondary OPs, basis vectors of the primitive cell and the change in the volume of a primitive cell (column "size"). Note that the sets of secondary OPs in the formation of P_I4_3 and P_I4_1 structures are the same. Symmetry analysis makes it possible to establish the physical realization of the secondary OPs: ferroelastic (*irrep* Γ_3^+) and nonferroelastic (*irreps* Γ_3^- and Γ_4^-) displacements of atoms [36, 42], as well as ordering (*irreps* Γ_3^+ and Γ_4^+) of d-orbitals [43].

The symmetry of predicted spin-ordered structures allows physical properties described by tensors of different orders (secondary ferroics) [32]. Table 2 lists some of these simple tensor properties, the irreducible representations by which they are converted, as well as the secondary order parameters from Table 1. Therefore, the predicted crystals are improper ferroics or type-II multiferroic materials. The analysis of the secondary OP (Table 1 and Table 2) shows that the improper ferroelectrics with the P_I4_3 and P_I4_1 structure can also be ferroelastic, ferroelastoelectric, ferrobielastic, ferrotoroidic and gyrotropic phases [44–47].

Spin ordering led to the formation of enantiomorphic (chiral) structures with P_I4_3 – and P_I4_1 – symmetries. They form an enantiomorphic pair. We see (Fig. 2) that the final P_I4_3 – and P_I4_1 – phases can be obtained in various symmetry ways from the initial phase. This conclusion corresponds to the so-called variable principle, which was first established in work [48]. From the initial structure with the $Fd\bar{3}m$ space group, this enantiomorphic pair is obtained through intermediate structures (Fig. 2). The intermediate structures, in turn, form two enantiomorphic pairs: $P4_122$ – $P4_322$ and $P4_12_12$ – $P4_32_12$. Enantiomorphic crystals modify one into another in mirror reflection. One of these modifications is

TABLE 2. Predicted improper physical properties of the crystals with P_I4_3 and P_I4_1 space group

Examples of physical properties or phenomena	Macro-parameters	Decomposition of reducible presentation	Secondary OPs from Table 1
Ferroelectric, polarization	Γ_4^-	Γ_4^-	$\Gamma_4^-\ (0,0,a)$
Ferroelastic, strain, stress, permitivity	$\left[\left(\Gamma_4^-\right)^2\right]$	$\Gamma_1^+ + \Gamma_3^+ + \Gamma_5^+$	$\Gamma_3^+(a,0)$
Longitudinal piezoelectric effect tensor	$\left[\left(\Gamma_4^-\right)^3\right]$	$\Gamma_2^- + 2\Gamma_4^- + \Gamma_5^-$	$\Gamma_4^-\ (0,0,a)$
Symmetric in all indices fourth-rank tensor, cubic susceptibility tensor neglecting dispersion	$\left[\left(\Gamma_4^-\right)^4\right]$	$2\Gamma_1^+ + 2\Gamma_3^+ + 2\Gamma_5^+ + \Gamma_4^+$	$\Gamma_3^+\ (a,0)$ $\Gamma_4^+\ (0,0,a)$
Ferroelastoelectric, piezoelectric tensor, electro-optic coefficient	$\left[\left(\Gamma_4^-\right)^2\right]\left(\Gamma_4^-\right)$	$\Gamma_2^- + \Gamma_3^- + 3\Gamma_4^- + 2\Gamma_5^-$	$\Gamma_3^-(0,a)$ $\Gamma_4^-\ (0,0,a)$
Ferrobielastic, electrostriction, elastooptic or piezooptic tensor	$\left[\left(\Gamma_4^-\right)^2\right]^2$	$3\Gamma_1^+ + \Gamma_2^+ + 4\Gamma_3^+ + 3\Gamma_4^+ + 5\Gamma_5^+$	$\Gamma_3^+\ (a,0)$ $\Gamma_4^+\ (0,0,a)$
Axial crystal	A	Γ_4^+	$\Gamma_4^+\ (0,0,a)$
Ferrotoroidic	$A\left(\Gamma_4^+\right)$	Γ_4^+	$\Gamma_4^+\ (0,0,a)$
Optical activity, gyration tensor	$\varepsilon\left[\left(\Gamma_4^-\right)^2\right]$	$\Gamma_1^- + \Gamma_3^- + \Gamma_5^-$	$\Gamma_1^-(a)$ $\Gamma_3^-(0,a)$
Enanthiomorphism, Pure gyrotropic phase	ε	Γ_1^-	$\Gamma_1^-(a)$
Gyrotropic ferroelastic	Γ_3^-	Γ_3^-	$\Gamma_3^-(0,a)$
Gyrotropic ferroelectric	Γ_4^-	Γ_4^-	$\Gamma_4^-\ (0,0,a)$

Explanations for Table 2. Γ_4^- – the vector representation of the $Fd\bar{3}m$ symmetry group, A – the axial representation of the $Fd\bar{3}m$ symmetry group, ε– pseudo scalar. Secondary OPs from Table 1 for primary OPs: $mX_3(0,0;0,0;a,0)$ + $mX_4(0,0;0,0;a,0)$ and $mX_3(0,0;0,0;0,a)$ +$mX_4(0,0;0,0;0,a)$ are the same.

conventionally called “right”, and the other - “left”. Enanthiomorphic objects are described by a point symmetry group containing only symmetry axes. Both forms of enantiomorphic crystals have optical activity (gyrotropes), but the crystal rotates the plane of polarization of light propagating along the optical axis, either along the left screw for one modification or the right screw for the other modification to the same angle.

However, the conditions for the existence of enaniomorphism do not completely coincide with the those for the existence of the optical activity. A novel functionality of enantiomorphic (chiral) materials is discovered in spintronics, which is known as “Chirality Induced Spin Selectivity” effect [49–52]. In our study, we established the opposite effect - the emergence of enantiomorphic (chiral) structures as a result of spin ordering associated with the lattice deformations and orbital ordering.

The symmetry allows trilinear coupling through mixed invariant $\gamma M_{mX_3} M_{mX_4} P_{\Gamma_4^-}$ in the thermodynamic potential, where γ is a coefficient characterizing the strength of the magnetoelectric coupling (by this invariant); M_{mX_3}, M_{mX_4} and $P_{\Gamma_4^-}$ are antiferromagnetic (M_{mX_3} and M_{mX_4}) and ferroelectric ($P_{\Gamma_4^-}$) OPs transformed according *irrep*s mX_3, mX_4

and Γ_4^-, respectively. Thus, space-inversion symmetry breaking the emergence of the spontaneous polarization results from the interaction between two antiferromagnetic orders, which do not separately lead to the ferroelectric distortion (Fig. 3). From the symmetry consideration, the emergence of spin-induced polarization in these phases is similar to the mechanism of the hybrid improper ferroelectricity in artificial superlattices ($PbTiO_3$/$SrTiO_3$ [13]) and Ruddlesden–Popper perovskite-like phases ($Ca_3Mn_2O_7$ [16]). But in these examples the linear polarization is the product of interaction between two types of the octahedron rotational modes (instead of the two types of antiferromagnetic OPs) through trilinear coupling term in the Landau thermodynamic potential. Thus, these theoretically predicted phases can be attributed to the multiferroics of type-II according to the Khomskii classification [2].

Considering a variety of spin-ordered pyrochlore-like compounds, we expect that they may be a potential arena for ferroaxial materials. Ferroaxial order is discussed as a new class of ferroic states in recent years [46, 53–55]. The so-called ferroaxial transitions (a transition from nonferroaxial to ferroaxial phases) are characterized by rotational structural distortions that break the mirror symmetry. Among the 32 crystallographic point groups, there are 13 ferroaxial (or pyroaxial) groups (1, $\overline{1}$, 2, m, $2/m$, 3, $\overline{3}$, 4, $\overline{4}$, $4/m$, 6, $\overline{6}$, and $6/m$ [56], among which there is a point group 4. In the ferroaxial state, clockwise and counterclockwise rotational distortions are energetically equivalent and form domain states whose spatial distributions have been reported recently [54–59]. However, transition $m\overline{3}m \rightarrow 4$ is not pure ferroaxial species because it accompanies ferroelectric, ferroelastic, gyrotropic transitions. Only a few ferroaxial materials that show a pure ferroaxial transition are reported to date [e.g., $RbFe(MoO_4)_2$ ($\overline{3}m \rightarrow \overline{3}$ at 190 K [60]) and $NiTiO_3$ ($\overline{3}m \rightarrow \overline{3}$ at 1560 K [61])].

We consider also gyrotropic phase transitions in which the initial phase is optically inactive or non-gyrotropic; Therefore, the ferroic optically active phase will be called the gyrotropic phase. The appearance of a spontaneous gyrotropic phase, which is not accompanied by either ferroelectricity or ferroelasticity, corresponds to the formation of so-called pure gyrotropic phase [47]. If the formation of a gyrotropic phase is accompanied by the appearance of polarization or deformation in the ferroic phase, then the optically active phase will be called gyrotropic ferroelectric or gyrotropic ferroelastic, respectively.

Thus, the predicted pyrochlore-like phases with P_I4_3 and P_I4_1 space symmetry are characterized by a complex and multi-order, including the structural, orbital, spin, optical, ferroaxial, ferrotoroidic, ferroelastoelectric, ferrobielastic, gyrotropic, electrical and other crystal freedom degrees.

4. Conclusions

In our work, we predict the possibility of the existence of two enantiomorphic multiferroics of type II with P_I4_3- and P_I4_1- symmetries, whose ferroelectrical properties appear as a result of magnetic ordering on the $16d$ Wyckoff positions in the initial $Fd\overline{3}m$ phase with pyrochlore sublattice(s). These multiferroics are objects to be searched and studied, since they can have not only magnetic and electrical properties, but, at the same time, they can have other above mentioned physical properties. This complex multi-order may result in unusual physical properties of the above materials.

References

[1] Vopson M.M. Fundamentals of Multiferroic Materials and Their Possible Applications. *Critical Reviews in Solid State and Materials Sciences*, 2014, **201**, P. 1–28.

[2] Khomskii D. Classifying multiferroics: Mechanisms and effects. *Physics*, 2009, **2**(20), P. 1-8.

[3] Selbach S.M., Tybell T., et al. The Ferroic Phase Transitions of $BiFeO_3$. *Adv. Mater.*, 2008, **20**, P. 3692–3696.

[4] Kimura T., Kawamoto S., et al. Magnetocapacitance effect in multiferroic $BiMnO_3$. *Phys. Rev. B*, 2003, **67**, P. 180401(1-4) (R).

[5] Seshadri R., Hill N. A. Visualizing the role of Bi $6s$ "lone pairs" in the off-center distortion in ferromagnetic $BiMnO_3$. *Chem. Mater.*, 2001, **13**, P. 2892–2899.

[6] Kimura T., Goto T., et al. Magnetic control of ferroelectic polarization. *Nature*, 2003, **426**, P. 55–58.

[7] Hur N., Park S., et al. Electric polarization reversal and memory in a multiferroic material induced by magnetic fields. *Nature*, 2004, **429**, P. 392–395.

[8] Cheong S.W., Mostovoy M. Multiferroics: a magnetic twist for ferroelectricity. *Nature Mater*, 2007, **6**, P. 13–20.

[9] Hill N. A. Why there are so few multiferroics with the perovskites structure? *J. Phys. Chem. B*, 2000, **104**(29), P. 6694–6709.

[10] Polinger V., Garcia-Fernandez P., et al. Pseudo Jahn–Teller origin of ferroelectric instability in $BaTiO_3$ type perovskites: The Green's function approach and beyond. *Physica B: Condensed Matter*, 2015, **457**, P. 296–309.

[11] Smolenskii G. A., Chupis I. E. Ferroelectromagnets. *Physics–Uspekhi*, 1982, **25**, P. 475–493.

[12] Nan C.-W. Multiferroic magnetoelectric composites: Historical perspective, status, and future directions. *J. Appl. Phys.*, 2008, **103**, P. 031101(1-35).

[13] Bousquet E., Dawber M., et al. Improper ferroelectricity in perovskite oxide artificial superlattices. *Nature*, 2008, **452**, P. 732–736.

[14] Sim H., Cheong S.W., et al. Octahedral tilting-induced ferroelectricity in $ASnO_3$/A'SnO_3 superlattices (A, A'=Ca, Sr, and Ba). *Phys. Rev. B*, 2013, **88**, P. 014101(1-7).

[15] Zhao H.J., Íñiguez J., et al. Atomistic theory of hybrid improper ferroelectricity in perovskites. *Phys. Rev. B*, 2014, **89**, P. 174101(1-7).

[16] Benedek N. A., Fennie C.J. Hybrid Improper Ferroelectricity: A Mechanism for Controllable Polarization-Magnetization Coupling. *Phys. Rev. Lett.*, 2011, **106**, P. 107204(1-4).

[17] Rondinelli J.M., Fennie C.J. Octahedral Rotation-Induced Ferroelectricity in Cation Ordered Perovskites. *Adv. Mater.*, 2012, **24**, P. 1961–1968.

[18] Mulder A.T., Benedek N.A., et al. Turning ABO_3 Antiferroelectrics into Ferroelectrics: Design Rules for Practical Rotation-Driven Ferroelectricity in Double Perovskites and $A_3B_2O_7$ Ruddlesden-Popper Compounds. *Adv. Func. Mater.*, 2013, **23**, P. 4810–4820.

[19] Benedek N.A., Rondinelli J.M., et al. Understanding ferroelectricity in layered perovskites: new ideas and insights from theory and experiments. *Dalton Trans.*, 2015, **44**, P. 10543–10558.
[20] Santos S.S.M., Marcondes M.L., et al. Spontaneous electric polarization and electric field gradient in hybrid improper ferroelectrics: insights and correlations. *J. Mater. Chem. C*, 2021, **22**, P. 15074–15082.
[21] Oh Y.S., Luo X., et al. Experimental demonstration of hybrid improper ferroelectricity and the presence of abundant charged walls in (Ca, Sr)$_3$Ti$_2$O$_7$ crystals. *Nature Mater.*, 2015, **14**, P. 407–413.
[22] Liu X.Q., Wu J.W., et al Direct observation of ferroelectricity in $Ca_3Mn_2O_7$ and its prominent light absorption. *Appl. Phys. Lett.*, 2015, **106**, P. 202903(1-5).
[23] Yoshida S., Akamatsu H., et al. Hybrid Improper Ferroelectricity in (Sr,Ca)$_3$Sn$_2$O$_7$ and Beyond: Universal Relationship between Ferroelectric Transition Temperature and Tolerance Factor in n = 2 Ruddlesden–Popper Phases. *J. Am. Chem. Soc.*, 2018, **140**, P. 15690–15700.
[24] Yoshida S., Fujita K., et al. Ferroelectric $Sr_3Zr_2O_7$: Competition between Hybrid Improper Ferroelectric and Antiferroelectric Mechanisms. *Adv. Funct. Mater.*, 2018, **30**, P. 1801856(1-12).
[25] Hu Z.Z., Lu J.J., et al First-order phase transition and unexpected rigid rotation mode in hybrid improper ferroelectric (La, Al) co-substituted $Ca_3Ti_2O_7$ ceramics. *J. Materiomics*, 2019, **5**, P. 618–625.
[26] Lee M.H., Chang C.-P., et al. Hidden Antipolar Order Parameter and Entangled Néel-Type Charged Domain Walls in Hybrid Improper Ferroelectrics. *Phys. Rev. Lett.*, 2017, **119**, P. 157601(1-6).
[27] Smith K.A., Nowadnick E.A., et al. Infrared nano-spectroscopy of ferroelastic domain walls in hybrid improper ferroelectric $Ca_3Ti_2O_7$. *Nature Commun.*, 2019, **10**, P. 5235(1-9).
[28] Boström H.L.B., Senn M.S., Goodwin A.L. Recipes for improper ferroelectricity in molecular perovskites. Nature Commun., 2018, **9**, P. 2380(1-7).
[29] Boström H.L.B., Goodwin A.L. Hybrid Perovskites, Metal–Organic Frameworks, and Beyond: Unconventional Degrees of Freedom in Molecular Frameworks. *Acc.Chem.Res.*, 2021, **54**, P. 1288–1297.
[30] Stroppa A., Barone P., et al. Hybrid Improper Ferroelectricity in a Multiferroic and Magnetoelectric Metal-Organic Framework. *Adv. Mater.*, 2013, **25**, P. 2284–2290.
[31] Tokura Y., Seki S. Multiferroics with Spiral Spin Orders. *Advanced Materials*, 2010, **22**(14), P. 1554–1565.
[32] Talanov M.V., Shirokov V.B., Pimenov M.S., Talanov V.M. Magnetic phase diagrams of the pyrochlore-based magnets: Landau theory. *J. Magn. Magn. Mat*, 2023 (in press).
[33] Choi Y.J., Yi H.T., et al. Ferroelectricity in an Ising Chain Magnet. *Phys. Rev. Lett.*, 2008, **100**, P. 047601(1-4).
[34] Arima T. Ferroelectricity induced by proper-screw type magnetic order, *J. Phys. Soc. Jpn.*, 2007, **76**, P. 073702(1-4).
[35] Talanov M.V., Talanov V.M. Structural Diversity of Ordered Pyrochlores. *Chem Mater.*, 2021, **33**, P. 2706–2725.
[36] Talanov M.V., Talanov V.M. Formation of Breathing Pyrochlore Lattices: Structural, Thermodynamic and Crystal Chemical Aspects. *CrystEngComm.*, 2020, **22**, P. 1176–1187.
[37] Campbell B.J., Stokes H.T., et al., ISODISPLACE: a web-based tool for exploring structural distortions. *J. Appl. Cryst.*, 2006, **39**, P. 607–614.
[38] Perez-Mato J., Gallego S., et al. Symmetry-Based Computational Tools for Magnetic Crystallography. *Annu. Rev. Mater. Res.*, 2015, **45**, P. 217–248.
[39] Momma K., Izumi F. VESTA: a three-dimensional visualization system for electronic and structural analysis. *J. Appl. Cryst*, 2008, **41**, P. 653–658.
[40] Belov N.V., Neronova N.N., Smirnova T.S. *Tr. Inst. Krist. Akad. SSSR.*, 1955, **11**, P. 33–67, English translation in *Sov. Phys. Crystallogr.*, 1957, **1**, P. 487–488.
[41] Campbell B.J., Stokes H.T., et al. Introducing a unified magnetic space-group symbol, *Acta Cryst. A*, 2022, **78**, P. 99–106.
[42] Talanov M.V., Talanov V.M. Order parameters and phase diagrams of ferroelastics with pyrochlore structure, *Ferroelectrics*, 2019, **543**, P. 1–11.
[43] Talanov M.V., Shirokov V.B., et al., Vanadium clusters formation in geometrically frustrated spinel oxide AlV_2O_4, *Acta Crystallogr. B*, 2018, **74**, P. 337–353.
[44] Sirotin Y.I. *Shaskol'skaya M.P. Foundations of Crystal Physics*. Nauka, Moscow, 1979.
[45] Tagantsev A.K., Cross L.E., Fousek J. *Domains in Ferroic Crystals and Thin Films*. Springer Science+Business Media, LLC, 2010, 821 p.
[46] Hlinka J., Privratska J., et al. Symmetry Guide to Ferroaxial Transitions. *Phys. Rev. Lett.*, 2016, **116**, P. 177602(1-6).
[47] Koňák Č., Kopský V., Smutný F. Gyrotropic phase transitions. *J. Phys. C: Solid State Phys.*, 1978, 11, P. 2493–2518.
[48] Talanov M.V. Group-theoretical analysis of 1:3 A-site-ordered perovskite formation. *Acta Cryst. A*, 2019, **75**, P. 379–397.
[49] Göhler B., Hamelbeck V., et al. Spin selectivity in electron transmission through self-assembled monolayers of double-stranded DNA. *Science*, 2011, **331**, P. 894–897.
[50] O. Ben Dor S. Yochelis, et al. Magnetization switching in ferromagnets by adsorbed chiral molecules without current or external magnetic field. *Nat. Commun.*, 2017, **8**, P. 14567(1-7).
[51] Naaman R., Paltiel Y., et al. Chiral Induced Spin Selectivity Gives a New Twist on Spin-Control in Chemistry. *Acc. Chem. Res.*, 2020, **53**, P. 2659–2667.
[52] Suda M., Thathong Y., et al. Light-driven molecular switch for reconfigurable spin filters. *Nat. Commun.*, 2019, **10**, P. 2455(1-7).
[53] Cheong S.-W., Talbayev, et al. Broken Symmetries. Non-reciprocity, and Multiferroicity. *npj Quantum Mater.*, 2018, **3**, P. 19.
[54] Jin, W., Drueke, E., et al. Observation of a Ferro-Rotational Order Coupled with Second-Order Nonlinear Optical Fields. *Nat. Phys.*, 2020, **16**, P. 42–46.
[55] Hayashida T., Uemura, et al. Visualization of Ferroaxial Domains in an Order-Disorder Type Ferroaxial Crystal. *Nat. Commun.*, 2020, **11**, P. 4582.
[56] Cheong S.-W., Lim S., et al. Permutable SOS (Symmetry Operational Similarity). *npj Quantum Mater*, 2021, *6*, P. 58.
[57] Hayami S., Oiwa R., Kusunose H. Electric Ferro-axial Moment as Nanometric Rotator as Source of Longitudinal Spin Current. *J. Phys. Soc. Jpn.*, 2022, **91**, P. 113702.
[58] Hayashida T., Uemura Y., et al. Phase Transition and Domain Formation in Ferroaxial Crystals. *Phys. Rev. Mater.*, 2021, *5*, P. 124409.
[59] Yokota H., Hayashida T., et al. Three dimensional Imaging of Ferroaxial Domains Using Circularly Polarized Second Harmonic Generation Microscopy. *npj Quantum Mater.*, 2022, *7*, P. 106.
[60] Waśkowska A. Gerward L., et al. Temperature-and pressure-dependent lattice behaviour of $RbFe(MoO_4)_2$. *J. Phys. Condens. Matter.*, 2010, *22*, P. 055406.
[61] Boysen H., Frey F., et al. Neutron Powder Investigation of the High-temperature Phase Transition in $NiTiO_3$. *Z. Kristallogr. – Cryst. Mater.*, 1995, *210*, P. 328–337.

Submitted 24 March 2023; revised 28 March 2023; accepted 29 March 2023

Information about the authors:

Valeriy M. Talanov – Platov South-Russian State Polytechnic University, Novocherkassk, Rostov region, 346428, Russia; ORCID 0000-0002-1269-2521; valtalanov@mail.ru

Mikhail V. Talanov – Platov South-Russian State Polytechnic University, Novocherkassk, Rostov region, 346428, Russia; Southern Federal University, Rostov-on-Don,344090, Russia; ORCID 0000-0002-5416-9579; mvtalanov@gmail.com

Vladimir B. Shirokov – Platov South-Russian State Polytechnic University, Novocherkassk, Rostov region, 346428, Russia; Southern Federal University, Rostov-on-Don,344090, Russia; Southern Scientific Center of Russian Academy of Sciences, Rostov-on-Don, 344006, Russia; ORCID 0000-0002-5267-2226; shirokov.ssc@gmail.com

Conflict of interest: the authors declare no conflict of interest.